Draft version September 9, 2016
Preprint typeset using LaTeX style AASTeX6 v. 1.0

A NEW ASTROBIOLOGICAL MODEL OF THE ATMOSPHERE OF TITAN

K. Willacy
MS 169-507, Caltech/Jet Propulsion Laboratory, 4800 Oak Grove Drive, Pasadena, CA 91109

M. Allen[1]
Caltech/Jet Propulsion Laboratory, 4800 Oak Grove Drive, Pasadena, CA 91109

Y. Yung
Division of Geological and Planetary Science, California Institute of Technology, Pasadena, CA 91125

[1]Division of Geological and Planetary Science, California Institute of Technology, Pasadena, CA 91125

ABSTRACT

We present results of an investigation into the formation of nitrogen-bearing molecules in the atmosphere of Titan. We extend a previous model (Li et al. 2014, 2015) to cover the region below the tropopause, so the new model treats the atmosphere from Titan's surface to an altitude of 1500 km. We consider the effects of condensation and sublimation using a continuous, numerically stable method. This is coupled with parameterized treatments of the sedimentation of the aerosols and their condensates, and the formation of haze particles. These processes affect the abundances of heavier species such as the nitrogen-bearing molecules, but have less effect on the abundances of lighter molecules. Removal of molecules to form aerosols also plays a role in determining the mixing ratios, in particular of HNC, HC_3N and HCN. We find good agreement with the recently detected mixing ratios of C_2H_5CN, with condensation playing an important role in determining the abundance of this molecule below 500 km. Of particular interest is the chemistry of acrylonitrile (C_2H_3CN) which has been suggested by Stevenson et al. (2015) as a molecule that could form biological membranes in an oxygen-deficient environment. With the inclusion of haze formation we find good agreement of our model predictions of acrylonitrile with the available observations.

Keywords: astrochemistry, planets and satellites: atmospheres, planets and satellites: composition, planets and satellites: individual (Titan)

1. INTRODUCTION

Karen.Willacy@jpl.nasa.gov

A major goal of planetary exploration is to obtain a fundamental understanding of planetary environments, both as they are currently and as they were in the past. This knowledge can be used to explore the questions of (a) how conditions for planetary habitability arose and (b) the origins of life. Titan is a unique object of study in this quest. Other than Earth itself, and Pluto (which has also been observed to have photochemically produced haze; Stern et al. 2015; Gladstone et al. 2016), Titan is the only solar system body demonstrated to have complex organic chemistry occurring today. Its atmospheric properties— (1) a thick N_2 atmosphere, (2) a reducing atmospheric composition, (3) energy sources for driving disequilibrium chemistry and (4) an aerosol layer for shielding the surface from solar UV radiation—suggest it is a counterpart of the early Earth, before the latter's reducing atmosphere was eradicated by the emergence and evolution of life (Coustenis & Taylor 1999; Lunine 2005; Lorenz & Mitton 2008).

A significant number of photochemical models have been developed to investigate the distribution of hydrocarbons in Titan's atmosphere (Strobel 1974; Yung et al. 1984; Lara et al. 1996; Wilson & Atreya 2004; De La Haye et al. 2008; Lavvas et al. 2008a,b; Krasnopolsky 2009). Recently, more constraints have been placed on the abundance of hydrocarbons and nitriles in the mesosphere of Titan (500 – 1000 km) from Cassini/UVIS stellar occultations (Koskinen et al. 2011; Kammer et al. 2013). In combination with the updated version of Cassini/ CIRS limb view (Vinatier et al. 2010), the complete profiles of C_2H_2, C_2H_4, C_6H_6, HCN, HC_3N are revealed for the first time. C_3 compounds, including C_3H_6, were modeled by Li et al. (2015), and the agreement with observations (Nixon et al. 2013) is satisfactory. The chemistry of many of these nitrogen molecules has recently been modeled by Loison et al. (2015).

In this paper we introduce our updated Titan chemical model that includes the formation of such potentially astrobiologically important molecules as acrylonitrile. In addition to the usual gas phase chemistry, it also includes a numerically stable treatment of the condensation and sublimation, allowing the formation and destruction of ices in the lower atmosphere to be tracked. Haze formation is also included in a parameterized fashion, allowing for the permanent removal of molecules from the atmosphere. We present here the effects of condensation on the nitrogen chemistry. The interaction of hydrocarbons and nitrile species in the condensed phase is complex and is beyond the scope of this paper (see, for example, Figures 1 and 2 of Anderson et al. 2016).

We begin with describing our updated model and in particular our treatment of condensation and sublimation (Section 2). We use this updated model to consider the chemistry in Titan's atmosphere from the surface of the moon to an altitude of 1500 km. We explore how condensation processes and haze formation affect the predicted gas phase abundances of observable molecules (Section 3). We also consider where the condensates form within the atmosphere (Section 2.2). Section 4 presents our conclusions.

2. THE MODEL

We use the Caltech/JPL photochemical model (KINETICS; Allen et al. 1981) with a recently updated chemical network, and with the addition of condensation and sublimation processes to explore the atmospheric chemistry of Titan. The 1-D model solves the mass continuity equation from the surface of Titan to 1500 km altitude:

$$\frac{\partial n_i}{\partial t} + \frac{\partial \psi_i}{\partial z} = P_i - L_i \tag{1}$$

where n_i is the number density of species i, and P_i and L_i are its chemical production and loss rates respectively. ψ_i is the vertical flux of i calculated from

$$\psi_i = -\frac{\partial n_i}{\partial z}(D_i + K_{zz}) - n_i\left(\frac{D_i}{H_i} + \frac{K_{zz}}{H_a}\right) - n_i\frac{\partial T}{\partial z}\frac{(1+\alpha_i)D_i + K_{zz}}{T} \tag{2}$$

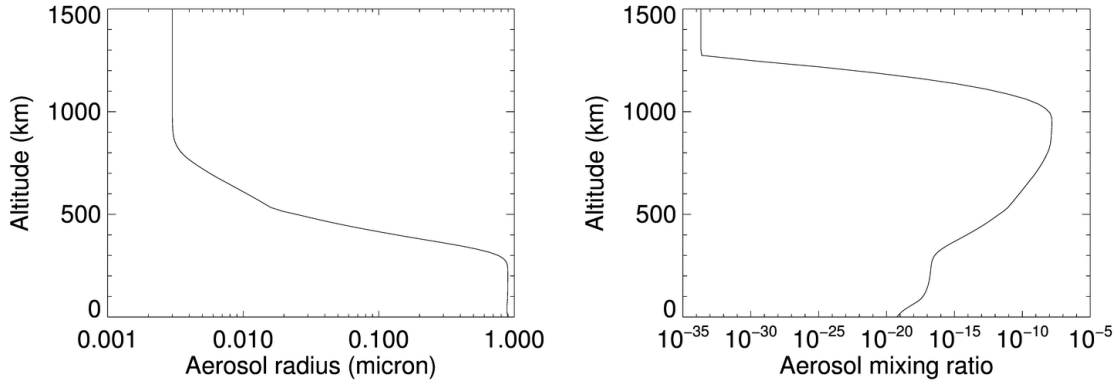

Figure 1. Aerosol properties from Lavvas et al. (2010) derived from a microphysical model validated against DISR observations. *left:* The mean radius of particles. *right:* The mixing ratio of particles.

where D_i and H_i are the molecular diffusion coefficient and the scale height for species i respectively, H_a is the atmospheric scale height, α_i is the thermal diffusion coefficient of species i, T is the temperature and K_{zz} is the eddy diffusion coefficient. The eddy diffusion coefficient used here is taken from Li et al. (2015) and can be summarized as

$$logK_{zz}(z) = \begin{cases} log(3\times10^3), & z < z_1 \\ log(3\times10^3)\dfrac{z_2-z}{z_2-z_1} + log(2\times10^7)\dfrac{z-z_1}{z_2-z_1}, & z_1 \le z < z_2 \\ log(2\times10^7)\dfrac{z_3-z}{z_3-z_1} + log(2\times10^6)\dfrac{z-z_2}{z_3-z_2}, & z_2 \le z < z_3 \\ log(2\times10^6)\dfrac{z_4-z}{z_4-z_3} + log(4\times10^8)\dfrac{z-z_3}{z_4-z_3}, & z_3 \le z < z_4 \\ log(4\times10^8), & z \ge z_4 \end{cases} \quad (3)$$

The atmospheric density and temperature profiles are also taken from Li et al. (2015), and are based on the T40 Cassini flyby (Westlake et al. 2011).

Aerosols are included in our model, both for the absorption of UV radiation and to provide surfaces onto which molecules can condense. The aerosol properties are from Lavvas et al. (2010) who derived them from a microphysical model validated against Cassini/Descent Imager Spectral Radiometer (DISR) observations. Their results provide the mixing ratio and surface area of aerosol particles as a function of altitude (Figure 1). To calculate the absorption of UV by dust we assume absorbing aerosols with extinction cross-sections that are independent of wavelength (Li et al. 2014, 2015).

2.1. *Boundary Conditions*

Family	Molecule
	H, H_2
hydrocarbons	C CH CH_2 $^3CH_2$ CH_3 CH_4 C2 C_2H C_2H_2 C_2H_3 C_2H_4 C_2H_5 C_2H_6 C_3 C_3H C_3H_2 C_3H_3 C_2CCH_2 CH_3C_2H C_3H_5 C_3H_6 C_3H_7 C_3H_8 C_4H C_4H_2 C_4H_3 C_4H_4 C_4H_5 1-C_4H_6 1,2-C_4H_6 1,3-C_4H_6 C_4H_8 C_4H_9 C_4H_{10} C_5H_3 C_5H_4 C_6H C_6H_2 C_6H_3 C_6H_4 C_6H_5 *l*-C_6H_6 C_6H_6 C_8H_2
nitrogen-molecules	N NH NH_2 NH_3 N_2H N_2H_2 N_2H_3 N_2H_4 CN HCN HNC H_2CN CHCN CH_2CN CH_3CN C_2H_3CN C_2H_5CN C_3H_5CN C_2N_2 HC_2N_2 C_3N HC_3N HC_4N CH_3C_2CN H_2C_3N C_4N_2 HC_5N C_6N_2 CH_2NH CH_2NH_2 CH_3NH CH_3NH_2
condensed molecules	$C_2H_2^c$ $C_2H_4^c$ $C_2H_6^c$ $CH_2CCH_2^c$ $CH_3C_2H^c$ $C_3H_6^c$ $C_3H_8^c$ $C_4H_2^c$ $C_4H_4^c$ 1-$C_4H_6^c$ 1,2-$C_4H_6^c$ 1,3-$C_4H_6^c$ $C_4H_8^c$ $C_4H_{10}^c$ $C_5H_4^c$ *l*-$C_6H_6^c$ $C_6H_6^c$ HCN^c HNC^c CH_3CN^c $C_2H_3CN^c$ $C_2H_5CN^c$ $C_3H_5CN^c$ $C_2N_2^c$ $C_4N_2^c$ $C_6N_2^c$ HC_3N^c HC_5N^c $CH_3C_2CN^c$ CH_2NH^c $CH_3NH_2^c$ NH_3^c $N_2H_2^c$ $N_2H_4^c$

Table 1. The species included in the model. A superscript of ^{c} indicates the molecule is condensed.

The lower boundary of our model is the surface of Titan and the upper boundary is at 1500 km. For H and H_2 the flux at the lower boundary is zero and at the top of the atmosphere these molecules are allowed to escape with velocities of 2.4×10^4 cms^{-1} and 6.1×10^3 cms^{-1} respectively (equivalent to fluxes of 3.78×10^8 H atoms cm^{-2} and 6.2×10^9 H_2 molecules cm^{-2}). For all other gaseous species the concentration gradient at the lower boundary is assumed to be zero, while they have zero flux at the top boundary. Observations suggest that CH_4 can escape from the top of the atmosphere by sputtering (de La Haye et al. 2007) but the same effect can be generated in models by applying a larger eddy diffusivity (Li et al. 2015, 2014; Yelle et al. 2008) which is the approach we have taken here. Condensed species have zero flux at both the upper and lower boundaries.

Table 1 provides a list of the molecules in our model. The mixing ratio of N_2 is set according to the observational data and held fixed, with values below 50 km taken from the Huygens observations (Niemann et al. 2005) and above 1000 km from Cassini/UVIS data (Kammer et al. 2013). Between 50 and 1000 km the mixing ratio is assumed to be 0.98. The mixing ratio of CH_4 is fixed to the observed (super-saturated) values (Niemann et al. 2010) below the tropopause and allowed to vary above this.

2.2. *Condensation and Sublimation*

Condensation occurs when the saturation ratio, S, of a molecule is greater than 1. S is defined as $n(x)/n_{sat}(s)$, where $n(x)$ is the gas phase mixing ratio of species x and $n_{sat}(x)$ is its saturated density derived from the saturated vapor pressure. For $S < 1$, condensation is switched off and sublimation of any adsorbed molecules can occur. The abrupt change in behavior at $S = 1$ can lead to numerical instabilities where the system oscillates between the condensation and sublimation regimes. In previous Titan models various methods have been used to smooth out the transition and prevent such instabilities. For example, Yung et al. (1984) parameterized the condensation rate in terms of S:

$$\text{Loss rate} \propto -\frac{S-1}{S} \tag{4}$$

This results in a relatively constant loss rate as a function of S. A more complicated expression was used by Lavvas et al. (2008a) to ensure that the loss rate increases with increasing saturation ratios:

$$\text{Loss rate} \propto -(S-1)\frac{exp(-0.5/ln(S+1)^2)}{ln(S+1)^2} \quad \text{for S} > 1 \tag{5}$$

Other expressions that have been invoked include

$$\text{Loss rate} \propto -lnS \tag{6}$$

(Krasnopolsky 2009).

Here we use a numerically stable method to determine the net condensation rate. The rate at which molecules condense on to a pre-existing aerosol particle is given by the collision rate with the particle:

$$k_c = \alpha_x \sigma v_x n(x) \quad \text{molecules s}^{-1} \tag{7}$$

where α is the sticking coefficient of molecule x (where $\alpha_x \leq 1$), σ is the collisional cross-section of the particles, v_x is the gas phase velocity of x, and $n(x)$ is its number density. For a pure ice the saturated vapor pressure is measured when the condensation and sublimation processes are in equilibrium. In this scenario

$$k_c n_{sat}(x) = k_s \Theta_x \tag{8}$$

where k_s is the sublimation rate and Θ_x is the surface coverage of molecule x. In the case of a pure ice, Θ_x = 1, and hence the sublimation rate, $k_s = k_c n_{sat}(x)$. The net condensation rate, J_c is therefore

$$J_c = \alpha_x \sigma v_x [n(x) - n_{sat}(x)\Theta_x] \quad \text{molecules s}^{-1} \tag{9}$$

When sublimation is taking place from a mixture of ices (rather than from pure ice) Θ will be less than 1 and the resulting gas phase abundance will be lower than the saturated value. Θ is calculated from

$$\Theta = n(x^c)/\Sigma_y n(y^c) \tag{10}$$

where $n(x^c)$ is the number density of x in the condensed phase, $\Sigma_y n(y^c)$ is the total number density of all molecules condensed on to the grain surface. We assume that the ices are well-mixed, so that the composition of the surface from which sublimation occurs reflects that of the bulk of the ice.

To determine the saturated densities used in this paper we use the expressions for the saturated vapor pressure given in Table 2. The values from these fits are extrapolated as necessary to provide saturation vapor pressures over a wider range of temperatures. Figure 2 compares the predicted mixing ratios of HCN and C_2H_2 with the value predicted directly from the saturated vapor pressure. It can be seen that the model produces good agreement with the saturation vapor pressure in regions where the gas is saturated.

2.3. *Sedimentation and Haze Formation*

We assume that the abundance, size and location of the aerosol particles is fixed. In reality the particles do not remain at the same altitude but rather sediment out towards the surface of Titan, taking any condensates with them. To mimic this effect we have included a loss process for condensed molecules which removes them from the model atmosphere with a rate coefficient of 10^{-10} s^{-1}. All condensed species are assumed to be lost at the same rate. The assumed size of this reaction rate is somewhat arbitrary and to test the sensitivity of our results to its value we also considered a loss rate of 10^{-12} molecules s^{-1}. Changing the rate was found to have no effect on the predicted gas phase mixing ratios.

In addition to the condensation of ice or liquids onto existing aerosols, molecules can also be incorporated into new or existing aerosols. In this scenario the molecules are then unavailable for return to the gas via

Molecule	Expression for log P_{sat} (mmHg)	Temp range (K)	Notes
CH_4	6.84570 - 435.6214/(T-1.639)	91 – 189	Yaws (2007)
C_2H_2	6.09748 - (1644.1/T) + 7.42346 log(1000./T)	80 – 145	Moses et al. (1992)
	7.3147 - 790.20947/(T-10.141)	192 – 208	Lara et al. (1996)
C_2H_4	1.5477 - 1038.1 (1/T - 0.011) + 16537./(1/T - 0.011)^2	77 – 89	Moses et al. (1992)
	8.724 - 901.6/(T-2.555)	89 –104	Moses et al. (1992)
	50.79 - 1703./T - 17.141 log(T)	104 – 120	Moses et al. (1992)
	6.74756 - 585./(T-18.18)	120 – 155	Moses et al. (1992)
C_2H_6	10.01 - 1085./(T - 0.561)	30 – 90	Lara et al. (1996)
	6.9534 - 699.10608/(T-12.736)	91 – 305	Yaws (2007)
CH_3C_2H	6.78485 - 803.72998/(T-43.92)	183 – 267	Yaws (2007)
CH_2CCH_2	6.62555 - 684.69623/(T-55.658)	144 – 294	Yaws (2007)
C_3H_6	6.8196 - 785./(T-26.)	161 – 241	Yaws (2007)
C_3H_8	7.0189 - 889.8642/(T-15.916)	85 – 176	Yaws (2007)
C_4H_2	5.3817 - 3300.5/T + 16.63415 $\log_{10}$(1000./T)	127–237	Lara et al. (1996)
	6.5326 - 761.68429/(T-74.732)	237 – 478	Yaws (2007)
C_4H_4	6.6633 - 826.0438/(T-59.712)	181 – 454	Yaws (2007)
1-C_4H_6	6.98198 - 988.75(T-39.99)	205 – 300	Yaws (2007)
1,2-C_4H_6	6.99383 - 1041.117/(T-30.726)	247 – 303	Yaws (2007)
1,3-C_4H_6	6.84999 - 930.546/(T-34.146)	215 – 287	Yaws (2007)
C_4H_8	6.8429 - 926.0998/(T-33.)	192 – 286	Yaws (2007)
C_4H_{10}	7.0096 - 1022.47681/(T-24.755)	135 – 425	Yaws (2007)
C_5H_4	7.986 - 1509.98716/(T-32.226)	234 – 367	Yaws (2007)
l-C_6H_6	7.95508 - 1773.77625/(T-52.937)	341 – 449	Yaws (2007)
C_6H_6	6.814 - 1090.43115/(T-75.852)	233 – 562	Yaws (2007)
NH_3	7.5874 - 1013.78149/(T-24.17)	196 – 405	Yaws (2007)
HCN	11.41 - 2318./T	132 – 168	Lara et al. (1996)
	8.0258 - 1608.28491/(T-286.893)	260 – 456	Yaws (2007)
HNC	11.41 - 2318./T	132 – 168	same as HCN
	8.0258 - 1608.28491/(T-286.893)	260 – 456	same as HCN
C_2N_2	6.9442 - 779.237/(T-60.078)	146 – 400	Yaws (2007)
C_4N_2	8.269 - 2155./T	147 – 384	Yaws (2007)
C_6N_2	8.269 - 2155./T	147 – 384	same as C_4N_2
HC_3N	6.2249 - 714.01178/(T-101.55)	214 – 315	Yaws (2007)
HC_5N	6.2249 - 714.01178/(T-101.55)	214 – 315	same as HC_3N
C_2H_3CN	7.8376 - 1482.7653/T-25.)	189 – 535	Yaws (2007)
C_2H_5CN	7.0414 - 1270.41907/(T-65.33)	204 – 564	Yaws (2007)
C_3H_5CN	7.0406 - 1617.87915/(T-34.032)	186 – 583	Yaws (2007)
N_2H_2	7.8288 - 1698.58081/(T-43.21)	270 – 653	same as N_2H_4
N_2H_4	7.8288 - 1698.58081/(T-43.21)	270 – 653	Yaws (2007)
CH_3NH_2	7.3638 - 1025.39819/(T-37.938)	180 – 430	Yaws (2007)
CH_3CN	6.8376 - 995.2049/(T-80.494)	266 – 518	Yaws (2007)
CH_3C_2CN	6.2249 - 714.01178/(T-101.855)	214 – 315	Yaws (2007)
CH_2NH	8.0913 - 1582.91077/(T-33.904)	175 –512	From Yaws (2007) value for CH_3OH

Table 2. Expressions used to calculate the saturated vapor pressures. In the absence of laboratory data we assume that the saturated vapor pressure of HNC is the same as HCN, and that of N_2H_2 is the same as N_2H_4. We follow Loison et al. (2015) in using the vapor pressure of CH_3OH for CH_2NH and in using H_3CN for H_5CN.

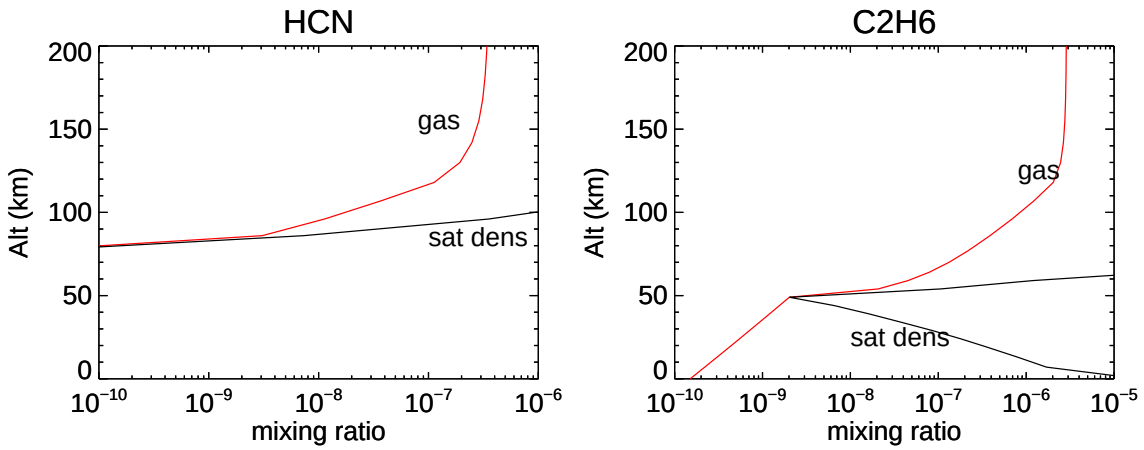

Figure 2. A comparison of the model results and the calculated mixing ratio under saturation conditions for (a) HCN and (b) C_2H_2. The saturated value (black line) is calculated assuming a pure ice and using the vapor pressure expressions given in Table 2. The model is shown in red. The two lines coincide in the region where the model calculations reach the saturated value and deviate where the calculated mixing ratios are below the saturated values.

sublimation and are permanently removed from the gas (Liang et al. 2007). This process is simulated using rates that are proportional to the collision rates between aerosols (assuming mean radii provided by Lavvas et al. (2010)) and molecules. We simulate this by adding reactions that remove the molecules from the gas with

$$\mathrm{X} + haze = haze \quad \mathrm{k} = \beta v \sigma n_g \ \mathrm{s}^{-1} \tag{11}$$

where n_g is the mixing ratio of aerosol particles, and β is an efficiency factor ranging from 0.01 to 10 depending on the molecule. The value of β was chosen for each molecule to maximize the agreement of the models with the observations. The molecules to be removed in this way are HCN (β = 0.01), C_2H_3CN (β = 0.1), HC_3N and HNC (β = 10) C_2H_5CN (β = 1). Other molecules are assumed not to condense in this way – for these molecules agreement of the models with observations is sufficiently good without invoking an additional loss mechanism such as haze formation.

3. RESULTS

3.1. *The Effect of Condensation Processes*

We present the results of three models with different assumptions about the condensation and sublimation. Model A is a gas phase only model, with no condensation. Model B includes condensation and sublimation processes as outlined in Section 2.2, and the sedimentation of aerosol particles and their condensates. Model C extends Model B to include the removal of molecules from the gas by haze formation. The model parameters are summarized in Table 3.

The largest effects are seen for the biggest molecules and in particular for those that contain nitrogen. The addition of sedimentation increases the rate of removal of these species from the gas in the lower atmosphere and improves agreement with the observations. However, some molecules are still found to be over-abundant. Further improvement is achieved between 200 and 600 km for HCN, HNC, HC_3N and C_2H_5CN if these molecules are assumed to be incorporated into haze particles.

Below we discuss the chemistry of several species in more detail.

Model	Condensation	Sedimentation	Haze formation
A	No	No	No
B	Yes	Yes	No
C	Yes	Yes	Yes

Table 3. Summary of model assumptions. Condensation and sublimation rates are discussed in Section 2.2. Sedimentation and haze formation rates are discussed in Section 2.3.

3.2. *Distribution of Nitrogen Molecules*

3.2.1. *NH_3*

In the lower atmosphere upper limits of the NH_3 abundance are provided by Herschel/SPIRE measurements (65 – 100 km; Teanby et al. 2013) and from CIRS/Cassini limb observations (110 – 250 km; Nixon et al. 2010). In the upper atmosphere the abundance is derived from Cassini/INMS of NH_4^+ (Vuitton et al. 2007) at 1100 km. Cui et al. (2009) claim a detection of NH_3 in the ionosphere between 950 and 1200km. Their value is an order of magnitude larger than that derived by Vuitton et al. and its origin is a matter of debate. It is possible that this high value is due to spent hydrazine fuel (Magee et al. 2009).

Our model abundances in the upper atmosphere are a factor of 10 lower than the observations of Vuitton et al. (2007) (Figure 3). Below 250 km our models are considerably lower (but consistent with) the upper limits derived by Teanby et al. (2013) and Nixon et al. (2010).

The main formation processes for NH_3 are

$$C_2H_3 + NH_2 \longrightarrow NH_3 + C_2H_2 \qquad < 800 \text{ km} \qquad (12)$$

with destruction by photodissociation.

As discussed by Loison et al. (2015) the formation of NH_3 via neutral-neutral reactions depends on the presence of NH_2 which is not efficiently produced in Titan's atmosphere. The inclusion of ion-molecule chemistry may lead to higher abundances of NH_3.

3.2.2. *HCN*

Observations of HCN have been made from 100 km to 1000 km. The millimeter observations of Marten et al. (2002) covered the whole disk and were mainly sensitive to the mid-latitude and equatorial regions. Observations from Cassini/CIRS (Vinatier et al. 2007, 2010), UVIS (Koskinen et al. 2011; Shemansky et al. 2005; Kammer 2015), and INMS (Magee et al. 2009) provide abundance information between 400 and 1000 km. Abundances in the lower atmosphere are also provided by Kim et al. (2005) from Keck observations (Geballe et al. 2003). Vervack et al. (2004) used Voyager 1 Ultraviolet Spectrometer measurements to determine abundances between 500 and 900km, although the inferred abundances are much higher than other estimates. The differences between the Voyager 1 HCN abundances and those from Cassini may be due to solar cycle variations. Investigating such differences is beyond the scope of this work.

Overall our models are in good agreement with the observational data (Figure 3). We find that condensation and sublimation are important for HCN below 500 km. The best fit to the observations is obtained with Model C (Figure 3), where sedimentation and haze formation reduce the abundance of HCN below 500 km.

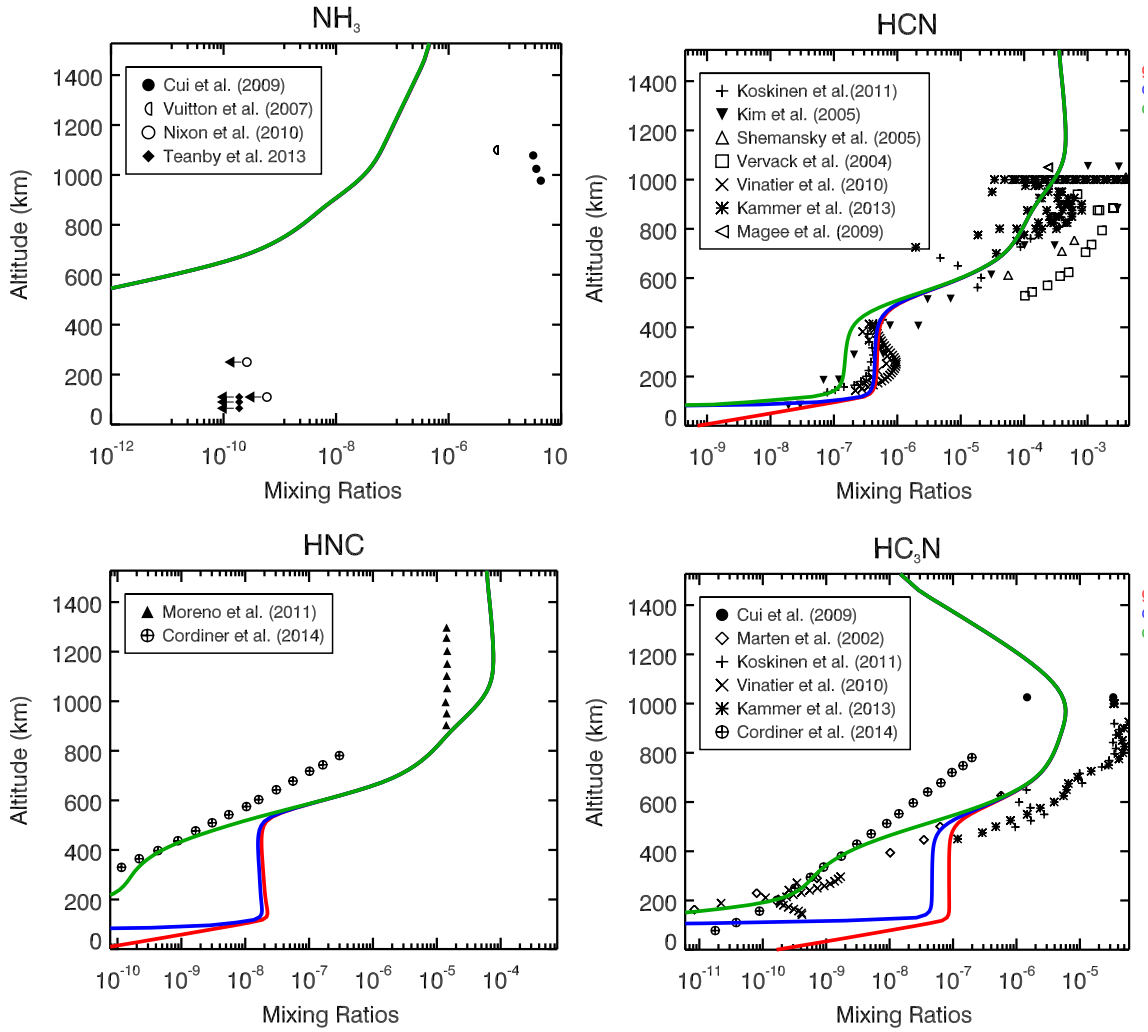

Figure 3. Distribution of some nitrogen-bearing molecules. (red line = Model A, blue line = Model B, green line = Model C). Cassini/INMS (● Cui et al. (2009); ◂ Magee et al. (2009), ◗ Vuitton et al. (2007)), Cassini/UVIS (+ Koskinen et al. (2011), ▵ Shemansky et al. (2005), ∗ Kammer (2015)), Keck (▼ Kim et al. 2005)), Voyager occultation observations (□ Vervack et al. (2004)), Cassini/CIRS (× Vinatier et al. (2010), ○Nixon et al. (2010), ◆ Teanby et al. (2013)), (▲ Moreno et al. 2011), IRAM (⋄ Marten et al. (2002)), ALMA (⊕ Cordiner et al. (2014)).

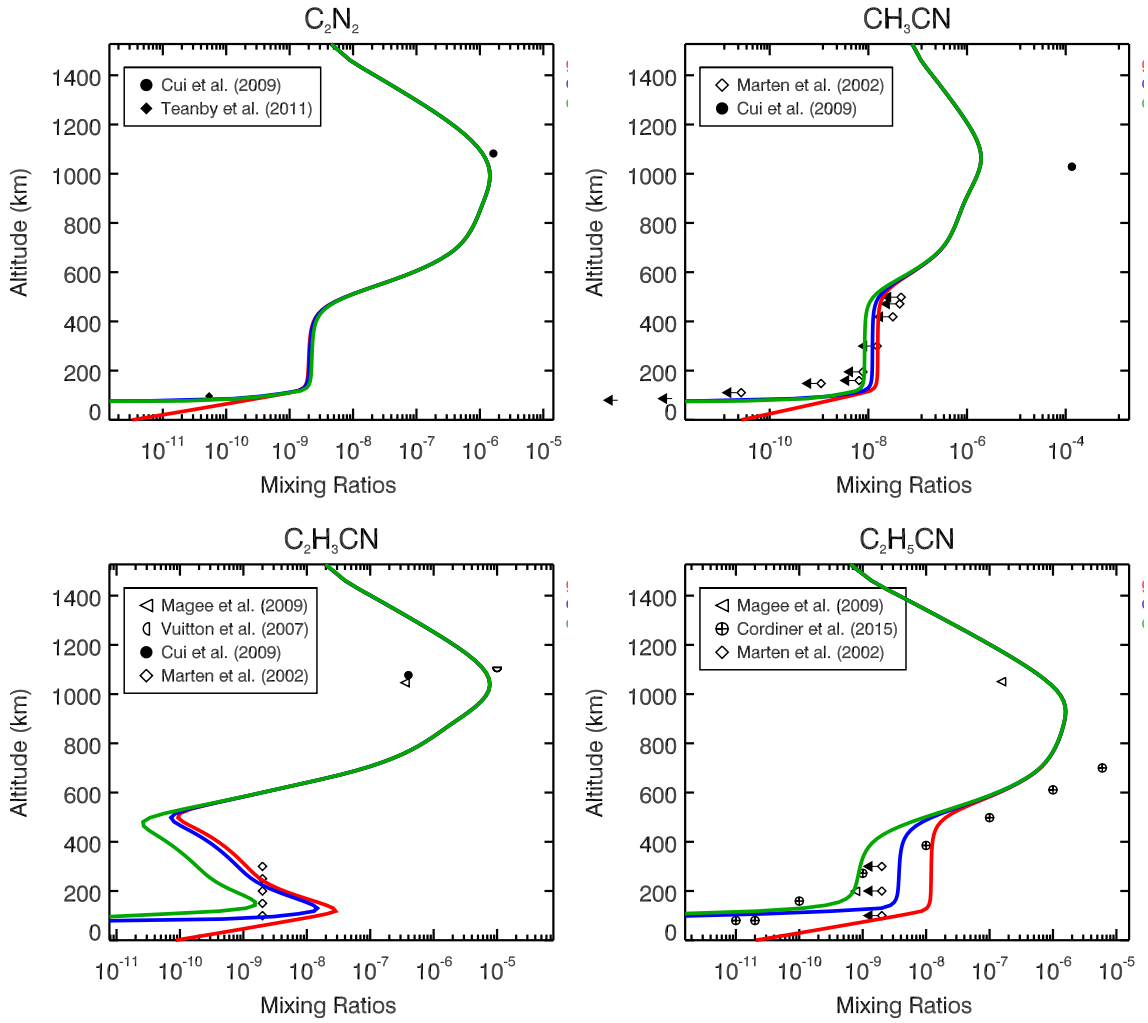

Figure 4. Abundances of more nitrogen-bearing species. Cassini/INMS (● Cui et al. (2009), ◁ Magee et al. (2009), ◖ Vuitton et al. (2007)), Cassini/CIRS (◆ Teanby et al. (2013)), IRAM 30m (◇ Marten et al. (2002)), ALMA data (⊕ Cordiner et al. (2015)).

The main formation processes are

$$\mathrm{HNC + H \longrightarrow HCN + H} \qquad 300 - 800\ \mathrm{km} \qquad (13)$$

$$\mathrm{CN + CH_4 \longrightarrow HCN + CH_3} \qquad 200 - 600\ \mathrm{km} \qquad (14)$$

$$\mathrm{N + CH_2 \longrightarrow HCN + H} \qquad 600 - 900\ \mathrm{km} \qquad (15)$$

$$\mathrm{C_2H_3CN} + h\nu \longrightarrow \mathrm{HCN + C_2H_2} \qquad < 1000\ \mathrm{km} \qquad (16)$$

$$\mathrm{H_2CN + H \longrightarrow HCN + H_2} \qquad 900 - 1300\ \mathrm{km} \qquad (17)$$

Photodissociation plays a role in both the formation of HCN (via photodisssociation of C_2H_3CN above

1000 km) and in its destruction (forming CN and H). Below 200 km destruction is by

$$C_2H_3 + HCN \longrightarrow C_2H_3CN + H \quad (18)$$

3.2.3. *HNC*

The first observations of HNC in Titan were made using Herschel/HIFI by Moreno et al. (2011). These measurements do not allow the exact vertical abundance profile to be determined. Several possible profiles can fit the data depending on the mixing ratio and the cut-off altitude assumed. Loison et al. (2015) suggest two possible profiles: one where the mixing ratio of HNC is 1.4 $\times 10^{-5}$ above 900 km (shown in Figure 3) and another where the mixing ratio is 6 $\times 10^{-5}$ above 1000 km. Our models fall between these two ranges.

More recently Cordiner et al. (2014) used ALMA to detect HNC. They found that the emission mainly originates at altitudes above 400 km and that there are two emission peaks that are not symmetrical in longitude. We are able to match their best fit profile reasonably well with model C (green line; Figure 3), where HNC forms haze providing the best agreement with the data at lower altitudes.

The main formation channels of HNC are

$$C_2H_3CN + h\nu \longrightarrow HNC + C_2H_2 \qquad < 900 \text{ km} \quad (19)$$

$$H_2CN + H \longrightarrow HNC + H_2 \qquad > 900 \text{ km} \quad (20)$$

$$N + CH_3 \longrightarrow HNC + H \qquad > 900 \text{ km} \quad (21)$$

The main destruction process is by reaction with H atoms forming HCN. This reaction has an activation barrier. In the literature the value for the activation barrier ranges from 800 to 2000 K (Talbi et al. 1996; Sumathi & Nguyen 1998; Petrie 2002; Wakelam et al. 2012). Here we are using the rate from the KIDA database (Wakelam et al. 2012) which has the highest activation barrier of 2000 K. Loison et al. (2015) used the lowest value (800 K), resulting in more efficient HCN production and consequently a lower gas phase abundance of HNC than we see here. We find that reducing the activation barrier does indeed reduce the mixing ratio of HNC but does not result in a good fit to the ALMA observations in this region (Figure 5).

3.2.4. *HC_3N*

HC_3N has been observed at altitudes from 200 to 1000 km (Marten et al. 2002; Vervack et al. 2004; Teanby et al. 2006; Vuitton et al. 2007; Cui et al. 2009; Magee et al. 2009; Vinatier et al. 2010; Cordiner et al. 2014). Below 500 km our models are in excellent agreement with the observations if it is assumed that HC_3N forms aerosols and thus is permanently removed from the gas (Figure 3 *(bottom left)*). Condensation and sublimation alone result in an over-estimate of the abundance compared to the observations in this region. Good agreement is also seen for all models between 500 km and 700 km. Above this our models tend to under predict the HC_3N abundance. Below 100 km the mixing ratio follows the saturation level, so that below this altitude the mixing ratio is much reduced compared to the gas only model. Better agreement with the observations below 400 km is obtained in the haze formation model where condensed molecules are assumed to be incorporated into aerosol particles and removed from the gas.

The main formation process below 1000 km is

$$C_3N + CH_4 \longrightarrow HC_3N + CH_3 \quad (22)$$

and above 800 km by

$$CN + C_2H_2 \longrightarrow HC_3N + H \quad (23)$$

$$C_2H_3CN + h\nu \longrightarrow HC_3N + H_2 \quad (24)$$

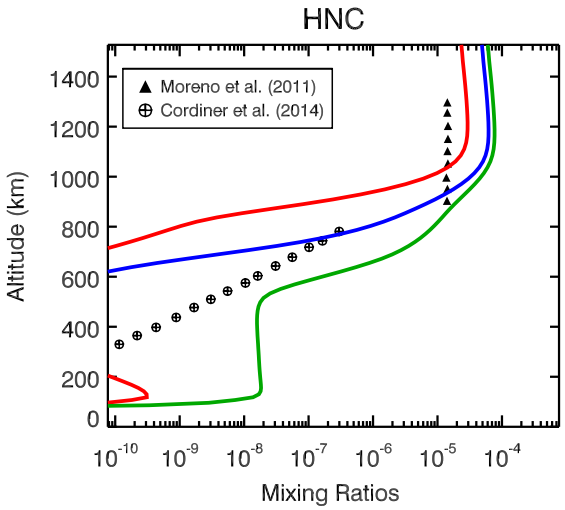

Figure 5. How the HNC abundance depends on the activation barrier of the reaction H + HNC ⟶ HCN + H. *green* E_A = 2000 K (Wakelam et al. 2012), *blue* E_A = 1400 K, *red* E_A = 800 K (Loison et al. 2015). The lower activation barrier results in more HNC being converted into HCN but does not result in a better agreement with the altitude distribution seen in the ALMA observations.

Destruction is by photodissociation

$$HC_3N + h\nu \longrightarrow C_3N + H \tag{25}$$

and by reaction with H atoms

$$H + HC_3N + M \longrightarrow H_2C_3N + M \tag{26}$$

The observations show a sharp decrease in the abundance of HC_3N below 400 km. In our models this can be accounted for if HC_3N is incorporated into haze particles (Model C). An alternative explanation of meridional circulation and condensation in the polar regions has been suggested (Loison et al. 2015; Hourdin et al. 2004).

3.2.5. C_2N_2

Observations of C_2N_2 have been made by Cassini/CIRS (Teanby et al. 2006, 2009) and by Cassini/INMS (Cui et al. 2009; Magee et al. 2009). The models with condensation are in very good agreement with both of these datasets (Figure 4). Without condensation the abundance in the lower atmosphere is over-estimated.

The main formation route for C_2N_2 is by the reaction of CN and HNC:

$$CN + HNC \longrightarrow C_2N_2 + H \tag{27}$$

with destruction via photodissociation forming CN or by

$$H + C_2N_2 + M \longrightarrow H_2CN_2 + M \quad < 400 \text{ km} \tag{28}$$

3.2.6. CH_3CN

Submillimeter observations with the IRAM 30 m telescope detected the CH_3CN (12-11) rotational line providing a disk average vertical profile up to 500 km, dominated by the equatorial region (Marten et al.

2002). Cassini/CIRS (Nixon et al. 2013) and Cassini/INMS (Vuitton et al. 2007; Cui et al. 2009) provide estimates of the abundance above 1000 km.

All models are in good agreement with the observations below 800 km, although all predict slightly lower abundances than observed between 500 and 600 km. The predicted mixing ratio at 1100 km is a factor of 10 lower than the observed value of 3 $\times 10^{-5}$ Cui et al. (2009).

The main formation processes are

$$CN + CH_4 \longrightarrow CH_3CN + H \qquad < 900 \text{ km} \qquad (29)$$

$$NH + C_2H_4 \longrightarrow CH_3N + H \qquad > 900 \text{ km} \qquad (30)$$

$$CH_2NH + CH = CH_3CN + H \qquad < 900 \text{ km} \qquad (31)$$

with destruction by

$$CH_3CN + H \longrightarrow CN + CH_4 \qquad < 1200 \text{ km} \qquad (32)$$

3.2.7. C_2H_3CN

Several observations have placed upper limits on the abundance of C_2H_3CN. Marten et al. (2002) used the IRAM 30m telescope to determine upper limits between 100 and 300 km. Cassini/INMS has provided an upper limit of 4 $\times 10^{-7}$ at 1077 km (Cui et al. 2009), while Cassini/INMS Magee et al. (2009) determined a mixing ratio of 3.5 $\times 10^{-7}$ at 1050 km and Vuitton et al. (2007) found 10^{-5} at 1100 km from observations of ions. Cordiner et al. (private communication) have detected C_2H_3CN in the submillimeter and found an average abundance of 1.9 x 10^{-9} above 300 km.The model abundance of C_2H_3CN in the upper atmosphere is within a factor of 2 of the Vuitton et al. (2007) value but 50 times higher than Magee et al. (2009) and Cui et al. (2009).

None of our models have a constant mixing ratio with altitude between 100 and 300 km as derived from the IRAM observations (Figure 4). Model B and C (which include condensation) are consistent with the derived mixing ratio at a particular altitude, but neither reproduce the constant value between 100 and 300 km. In the upper atmosphere all models predict mixing ratios within a factor a 3 of the Magee et al. (2009) result but are over-abundant compared to the other measurement in this region.

The main production mechanism is by reaction of CN with C_2H_4:

$$C_2H_3 + HCN \longrightarrow C_2H_5CN + H \qquad < 200 \text{ km} \qquad (33)$$

$$CN + C_2H_4 \longrightarrow C_2H_3CN + H \qquad 400 - 800 \text{ km} \qquad (34)$$

$$H_2C_3N + H \longrightarrow C_2H_3CN \qquad > 400 \text{ km} \qquad (35)$$

Gas phase destruction processes are

$$C_2H_3CN + h\nu \longrightarrow \begin{cases} HCN + C_2H_2 \\ HNC + C_2H_2 \\ HC_3N + H_2 \end{cases} \qquad (36)$$

Below 400 km haze formation and sedimentation of aerosol particles play an important role in determining the gas mixing ratio in Model C.

3.2.8. C_2H_5CN

Upper limits for the abundance of C_2H_5CN have been determined between 100 and 300 km from IRAM 30m observations Marten et al. (2002), with abundances in the upper atmosphere provided by Cassini/INMS data (Vuitton et al. 2007; Cui et al. 2009; Magee et al. 2009). More recently Cordiner et al. (2015) detected this molecule above 200 km using ALMA.

Our models over-estimate the abundance of C_2H_5CN in the upper atmosphere (Figure 4), probably because we do not include ion chemistry (for a discussion of this point see Loison et al. 2015). Below 700 km, Model C is in excellent agreement with the ALMA data of Cordiner et al.

The main formation process is

$$CH_2CN + CH_3 + M \longrightarrow C_2H_5CN + M \tag{37}$$

Destruction is by photodissociation

$$C_2H_5CN + h\nu \longrightarrow \begin{cases} C_2H_4 + HCN \\ CH_3 + CH_2CN \\ C_2H_3CN + H_2 \end{cases} \tag{38}$$

or by reaction with CH, C_2H_3 or C_2H.

$$C_2H_5CN + CH \longrightarrow CH_2CN + C_2H_4 \tag{39}$$

$$C_2H_5CN + C_2H \longrightarrow HC_3N + C_2H_5 \qquad < 300 \text{ km} \tag{40}$$

$$C_2H_3CN + C_2H_3 \longrightarrow C_2H_3CN + C_2H_5 \qquad < 300 \text{ km} \tag{41}$$

3.3. *Condensates in Titan's Atmosphere*

We find several layers at which condensates are abundant with the location being molecule dependent. The first condensate layer is in the lower atmosphere around the tropopause. Here we find condensates of C_2H_2, C_2H_4, C_2H_6, C_3H_8 among others. A little further up in the atmosphere around 65 – 80 km several molecules have peaks in condensation e.g. HCN, C_4H_8, C_4H_2, C_2H_3CN, C_2N_2, CH_3C_2H. Another layer of C_2H_3CN, CH_3CN, C_2H_5CN and CH_3C_2H forms around 110 – 130 km. Several molecules also have high condensation levels between 600 and 900 km e.g. CH_3C_2H, HC_5N, HC_3N, CH_3CN, and C_2H_5CN. Figure 6 shows the condensation layers for HCN and HC_3N. Both these molecules have high condensate abundances between 70 and 100 km, but HC_3N has a further peak around 500 km where the atmospheric temperature dips, and the gas phase abundance of this molecule is high.

The net flux of material falling on to the surface of Titan can be calculated from the difference between the atmospheric formation and destruction. Table 4 presents our predictions of the surface flux of nitrogen molecules. These are in solid form and if evenly distributed across Titan's surface would create a layer 4.4 m deep over a timescale of 1 Gyr. This amount of "fixed nitrogen" could be of biological importance.

4. DISCUSSION AND CONCLUSIONS

The removal of molecules by condensation plays an important role in determining the gas phase composition of Titan's atmosphere, as well as creating new aerosols. Condensates are found throughout the atmosphere. For the majority of molecules, condensation is most efficient below the tropopause. Larger molecules, and in particular nitrogen-bearing molecules have another condensation peak between 200 and 600 km. Relatively high abundances of condensates can also be present above 500 km if the gas phase abundance of a given molecule is high, e.g. HC_3N, HC_5N, CH_3CN and C_2H_5CN. These molecules condense

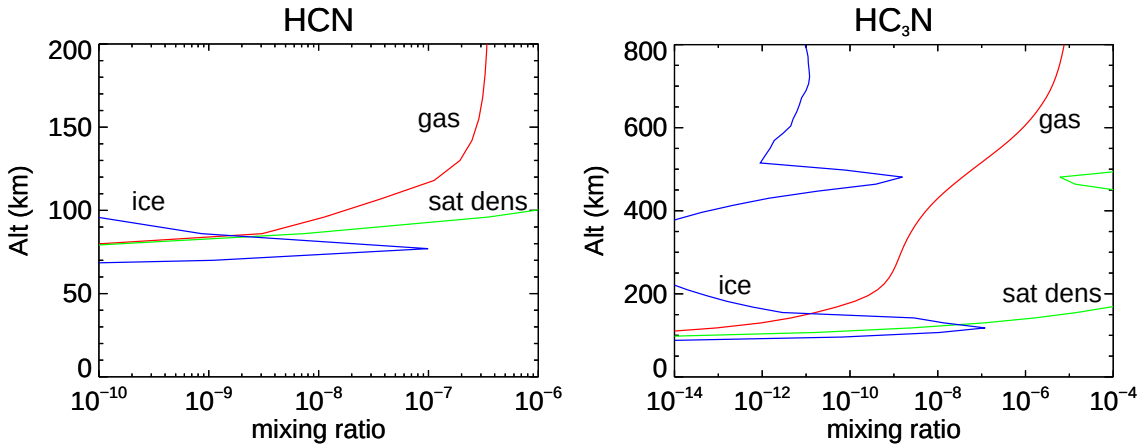

Figure 6. The calculated mixing ratios of HCN (left) and HC_2N (right) in the gas (red line) and in condensed form (blue line). Also shown is the saturated mixing ratio (green line). The mixing ratio of HCN^c peak at ~ 65 km. The mixing ratio of HCN in the gas around this altitude is slightly below the saturated value, even though there is condensed HCN available to be sublimated. The reason for this is that the condensates are not pure. Since the sublimation rate depends on the surface coverage of the condensed molecule sublimation from a mixed condensate is less efficient than from a pure condensate, leading to lower gas abundances. A similar effect is seen for other condensed molecules. For HC_3N the peak condensate mixing ratio occurs around 500 km where there is a dip in temperature corresponding to a high local abundance of HC_3N. Other nitrogen-bearing molecules show similar behavior in this region.

Molecule	Flux (molecules cm^{-2} s^{-1})	Flux (g cm^{-2}/Gyr)	Depth (m)	Solid/Liquid at 95 K
HCN^c	-1.2 ×10^8	-170	2.12	S
HNC^c	-8.1 ×10^6	-11.0	0.14	S
HC_3N^c	-2.9 ×10^7	-77.4	1.0	S
HC_5N^c	-3.4 10^6	-13.5	0.17	
$C_2N_2^c$	-5.8 ×10^5	-15.8	0.02	S
CH_3CN^c	-2.8 ×10^5	-0.6	0.01	S
CH_3C_2CN	-4.5 ×10^6	-15.3	0.19	
$C_2H_5CN^c$	-6.4 ×10^6	-18.4	0.23	S
$C_2H_3CN^c$	-1.5 ×10^7	-41.6	0.52	S
Total N			4.4 m	

Table 4. Flux of condensed molecules onto Titan's surface. Also shown are the estimated deposit thickness (depths) calculated assuming an average density of 0.8 g cm^{-3}.

in the region where Titan's haze forms. The effect is enhanced if it is assumed that some molecules can be permanently removed from the gas by being incorporated into aerosol particles. This mechanism was able to bring the abundances of HC_3N, HCN, HNC, CH_3CN and C_2H_5CN into good agreement with the observations below 600 km.

Although Titan possesses a rich organic chemistry it is unclear whether this could lead to life. Photochemically produced compounds on Titan, principally acetylene, ethane and organic solids, would release

energy when consumed with atmospheric hydrogen, which is also a photochemical product. McKay & Smith (2005) speculate on the possibility of widespread methanogenic life in liquid methane on Titan. On Earth fixed nitrogen is often a limiting nutrient. Our work shows that an abundant supply of fixed nitrogen, including species of considerable complexity, is available from atmospheric photochemistry.

Creating the kinds of lipid membranes that form the basis of lie on Earth depends on the presence of liquid water. Titan's atmosphere contains little oxygen and the surface temperature is well below that at which liquid water can survive. Instead surface liquids are hydrocarbons (e.g. Hayes 2016). Therefore any astrobiological processes, if present, are likely to be quite different to those on Earth. A recent paper by Stevenson et al. (2015) suggests that as alternative to lipids, membranes could be formed from small nitrogen-bearing organic molecules such as acrylonitrile (C_2H_3CN). Stevenson et al. calculate that a membrane composed of acrylonitrile molecules would be thermodynamically stable at cryogenic temperatures and would have a high energy barrier to decomposition.

All of our models predict abundances of C_2H_3CN that are in agreement with observations above 500 km. Below this condensation and incorporation into haze are required to bring the predicted mixing ratios down to the values inferred from observations Cordiner et al. (2015). If acrylonitrile were to be involved in life formation it needs to reach the surface of Titan. Our predicted flux of this molecule onto Titan's surface is 1.5×10^7 molecules cm^{-2} s^{-1}, or ~ 41.5 gcm^{-2}/Gyr, a quantity that is potentially of biological importance.

ACKNOWLEDGEMENTS

This research was conducted at the Jet Propulsion Laboratory, California Institute of Technology under contract with the National Aeronautics and Space Administration. Support was provided by the NASA Astrobiology Institute/Titan as a Prebiotic Chemical System. YLY was supported in part by the Cassini UVIS program via NASA grant JPL.1459109 to the California Institute of Technology. The authors thank Dr. Run-Lie Shia for his assistance with the KINETICS code and Dr. Panyotis Lavvas for providing the aerosol data used in these models.

REFERENCES

Allen, M., Yung, Y. L., & Waters, J. W. 1981, J. Geophys. Res., 86, 3617
Anderson, C. M., Samuelson, R. E., Yung, Y. L., & McLain, J. L. 2016, Geophys. Res. Letts., 43, 3088
Cordiner, M. A., Nixon, C. A., Teanby, N. A., et al. 2014, Astrophys. J. Letts, 795, L30
Cordiner, M. A., Palmer, M. Y., Nixon, C. A., et al. 2015, Astrophys. J. Letts, 800, L14
Coustenis, A., & Taylor, F. 1999, Titan : the earth-like moon (Singapore: World Scientific)
Cui, J., Yelle, R. V., Vuitton, V., et al. 2009, Icarus, 200, 581
De La Haye, V., Waite, J. H., Cravens, T. E., Robertson, I. P., & Lebonnois, S. 2008, Icarus, 197, 110
de La Haye, V., Waite, J. H., Johnson, R. E., et al. 2007, Journal of Geophysical Research (Space Physics), 112, A07309
Geballe, T. R., Kim, S. J., Noll, K. S., & Griffith, C. A. 2003, Astrophys. J. Letts, 583, L39
Gladstone, G. R., Stern, S. A., Ennico, K., et al. 2016, Science, 351, aad8866
Hayes, A. G. 2016, Annual Review of Earth and Planetary Sciences, 44, 57
Hourdin, F., Lebonnois, S., Luz, D., & Rannou, P. 2004, Journal of Geophysical Research (Planets), 109, E12005
Kammer, J. A. 2015, PhD thesis, California Institute of Technology
Kammer, J. A., Shemansky, D. E., Zhang, X., & Yung, Y. L. 2013, Planet. Space Sci., 88, 86
Kim, S. J., Geballe, T. R., Noll, K. S., & Courtin, R. 2005, Icarus, 173, 522
Koskinen, T. T., Yelle, R. V., Snowden, D. S., et al. 2011, Icarus, 216, 507
Krasnopolsky, V. A. 2009, Icarus, 201, 226
Lara, L. M., Lellouch, E., López-Moreno, J. J., & Rodrigo, R. 1996, J. Geophys. Res., 101, 23261
Lavvas, P., Yelle, R. V., & Griffith, C. A. 2010, Icarus, 210, 832
Lavvas, P. P., Coustenis, A., & Vardavas, I. M. 2008a, Planet. Space Sci., 56, 27
—. 2008b, Planet. Space Sci., 56, 67

Li, C., Zhang, X., Gao, P., & Yung, Y. 2015, Astrophys. J. Letts, 803, L19
Li, C., Zhang, X., Kammer, J. A., et al. 2014, Planet. Space Sci., 104, 48
Liang, M.-C., Yung, Y. L., & Shemansky, D. E. 2007, Astrophys. J. Letts, 661, L199
Loison, J. C., Hébrard, E., Dobrijevic, M., et al. 2015, Icarus, 247, 218
Lorenz, R., & Mitton, J. 2008, Titan Unveiled: Saturn's Mysterious Moon Explored (Princeton University Press)
Lunine, J. I. 2005, in Meteorites, Comets and Planets: Treatise on Geochemistry, ed. A. M. Davis (Elsevier B), 623
Magee, B. A., Waite, J. H., Mandt, K. E., et al. 2009, Planet. Space Sci., 57, 1895
Marten, A., Hidayat, T., Biraud, Y., & Moreno, R. 2002, Icarus, 158, 532
McKay, C. P., & Smith, H. D. 2005, Icarus, 178, 274
Moreno, R., Lellouch, E., Lara, L. M., et al. 2011, Astron. Astrophys., 536, L12
Moses, J. I., Allen, M., & Yung, Y. L. 1992, Icarus, 99, 318
Niemann, H. B., Atreya, S. K., Bauer, S. J., et al. 2005, Nature, 438, 779
Niemann, H. B., Atreya, S. K., Demick, J. E., et al. 2010, J. Geophys. Res. (Planets), 115, 12006
Nixon, C. A., Achterberg, R. K., Teanby, N. A., et al. 2010, Faraday Discussions, 147, 65
Nixon, C. A., Jennings, D. E., Bézard, B., et al. 2013, Astrophys. J. Letts, 776, L14
Petrie, S. 2002, J. Phys. Chem. A, 106, 11181
Shemansky, D. E., Stewart, A. I. F., West, R. A., et al. 2005, Science, 308, 978
Stern, S. A., Bagenal, F., Ennico, K., et al. 2015, Science, 350, aad1815
Stevenson, J., Lunine, J., & Clancy, P. 2015, Science Advances, 1, 1400067
Strobel, D. F. 1974, Icarus, 21, 466
Sumathi, R., & Nguyen, M. 1998, J. Phys. Chem. A, 102, 80138020
Talbi, D., Ellinger, Y., & Herbst, E. 1996, A&A, 314, 688
Teanby, N. A., Irwin, P. G. J., de Kok, R., et al. 2009, Icarus, 202, 620
—. 2006, Icarus, 181, 243
Teanby, N. A., Irwin, P. G. J., Nixon, C. A., et al. 2013, Planet. Space Sci., 75, 136
Vervack, R. J., Sandel, B. R., & Strobel, D. F. 2004, Icarus, 170, 91
Vinatier, S., Bézard, B., Fouchet, T., et al. 2007, Icarus, 188, 120
Vinatier, S., Bézard, B., Nixon, C. A., et al. 2010, Icarus, 205, 559
Vuitton, V., Yelle, R. V., & McEwan, M. J. 2007, Icarus, 191, 722
Wakelam, V., Herbst, E., Loison, J.-C., et al. 2012, Astrophys. J. Suppl., 199, 21
Westlake, J. H., Bell, J. M., Waite, Jr., J. H., et al. 2011, J. Geophys. Res. (Space Phys.), 116, 3318
Wilson, E. H., & Atreya, S. K. 2004, J. Geophys. Res., 106, 2181
Yaws, C. L. 2007, Yaws handbook of vapor pressures: Antoine Coefficients (Houston, Tex: Gulf Pub.)
Yelle, R. V., Cui, J., & Müller-Wodarg, I. C. F. 2008, Journal of Geophysical Research (Planets), 113, E10003
Yung, Y. L., Allen, M., & Pinto, J. P. 1984, Astrophys. J. Suppl., 55, 465